

Estimation of the mass outflow rates from viscous accretion discs

Rajiv Kumar^{1*}, Indranil Chattopadhyay¹

¹*Aryabhata Research Institute of Observational Sciences (ARIES), Manora Peak, Nainital – 263129, India*

Accepted —. Received —; in original form —

ABSTRACT

We study viscous accretion disc around black holes, and all possible accretion solutions, including shocked as well as shock free accretion branches. Shock driven bipolar outflows from a viscous accretion disc around a black hole has been investigated. One can identify two critical viscosity parameters α_{cl} and α_{cu} , within which the stationary shocks may occur, for each set of boundary conditions. Adiabatic shock has been found for upto viscosity parameter $\alpha = 0.3$, while in presence of dissipation and massloss we have found stationary shock upto $\alpha = 0.15$. The mass outflow rate may increase or decrease with the change in disc parameters, and is usually around few to 10 % of the mass inflow rate. We show that for the same outer boundary condition, the shock front decreases to a smaller distance with the increase of α . We also show that the increase in dissipation reduces the thermal driving in the post-shock disc, and hence the mass outflow rate decreases upto a few %.

Key words: hydrodynamics, black hole physics, accretion, accretion discs, jets and outflows

1 INTRODUCTION

One of the curious thing about the galactic as well as extra galactic black hole candidates is that, they show moderate to strong jets. Since black holes are compact and do not have hard surfaces, outflows and jets can originate only from the accreting material. And observations have indeed showed that the persistent jet or outflow activities are correlated with the hard spectral states of the disc *i.e.*, when the power radiated maximizes in the hard non-thermal part of the spectrum (Gallo et. al. 2003). Moreover, there seems to be enough evidence that these jets are produced within 100 Schwarzschild radius of the central object (Junor *et al.* 1999). So accretion disc models which are to be considered for persistent jet generation should allow the formation of jet close to the central object, and that the spectra of the disc should be in the hard state.

One of the most widely used accretion disc model — the Keplerian disc (Shakura & Sunyaev 1973; Novikov & Thorne 1973), is very successful in explaining the multicoloured black body part of the spectrum. However, the presence of Keplerian disc alone is inadequate in explaining the existence of the non-thermal tail of the spectrum. Moreover, the advection term in the equation of motion is poorly handled in this model, where the inner

disc was chopped off adhoc, and cannot automatically explain jet generation mechanism, neither can it explain the relative small size of the jet base. Hence, one has to consider accretion models which have significant advection. An elegant summary of all types of viscous accretion disc model has been provided by Lee *et al.* (2011). For the sake of completeness, we present a very brief account of advective discs, in the following.

Accretion onto black hole is necessarily transonic since radial velocity can only be small far away from the black hole, but matter must cross the horizon with velocity equal to the speed of light (c). Hence accretion solutions around black holes should consider the advection term self consistently. Accretion solution like Bondi flow or, radial flow (Bondi 1952; Chattopadhyay & Ryu 2009) although satisfies the transonicity criteria, but is of very low luminosity. Therefore, there was a need to consider rotating flow which are transonic too, such that the infall timescale would be long enough to generate the photons observed from microquasars and AGNs. The accretion model with advection which got wide attention, was ADAF (Ichimaru 1977; Narayan & Yi 1994). Initially ADAF was constructed around a Newtonian gravitational potential, where the viscously dissipated energy is advected along with the mass, and the momentum of the flow. The original ADAF solution was self-similar and wholly subsonic, thus violating the inner boundary condition around a black hole. This inadequacy was re-

* E-mail: rajiv.k@aries.res.in (RK); indra@aries.res.in (IC)

stored when global solutions of ADAF in presence of strong gravity showed that the flow actually becomes transonic at around few Schwarzschild radii (r_g), while remains subsonic elsewhere. The self-similarity of such a solution may be maintained far away from the sonic point (Chen *et al.* 1997). Moreover, the Bernoulli parameter is positive making the solutions unbound. This prompted the introduction of self-similar outflows in the ADAF abbreviated as ADIOS, which would carry away mass, momentum and energy (Blandford & Begelman 1999). Although this is an interesting addition to the generalization of ADAF type solutions, no physical mechanism was identified except the positivity of Bernoulli parameter of the accretion flow, that would drive these outflows.

Simultaneous to the research on ADAF class of solutions, a lot of progress was being made in the research of general advective, rotating solutions. For rotating advective flow, Liang & Thompson (1980) showed that with the increase in angular momentum of the inviscid flow, the number of physical critical points increases from one to two, and later it was shown that a standing shock can exist in between the two critical points (Fukue 1987; Chakrabarti 1989; Fukumura & Kazanas 2007; Chattopadhyay 2008; Chattopadhyay & Chakrabarti 2011). Since the accretion shock is centrifugal pressure mediated, there was apprehension about the stability and formation of such shocks, in presence of processes such as viscosity, which transports angular momentum outwards. All doubts about the stability of such shocks in presence of viscosity was subsequently removed (Lanzafame *et al.* 1998; Chakrabarti 1996; Chakrabarti & Das 2004; Chattopadhyay & Das 2007; Das & Chattopadhyay 2008; Lee *et al.* 2011). Furthermore, Fukumura & Tsuruta (2004) conjectured about the existence of multiple shocks and later, independent numerical simulations serendipitously found the existence of transient multiple shocks in presence of Shakura Sunyaev type viscosity (Lanzafame *et al.* 2008; Lee *et al.* 2011). Although, both general advective and ADAF solutions start with the same set of equations, it was intriguing that there can be two mutually exclusive class of solutions, and without any knowledge under which condition these solutions may arise. Lu *et al.* (1999) later showed that the global ADAF solution is a subset of general advective solutions. In other words, the models which concentrate only on the regime where the gravitational energy is converted mainly to the thermal and rotational energy, may either be cooling dominated (*e.g.*, Keplerian disc; Shakura & Sunyaev, 1973; Novikov & Thorne, 1973) or advection dominated (Narayan *et al.* 1997). Either way, these models remain mainly subsonic (except very close to the black hole) and hence do not show shock transition. However, if the entire parameter space is searched, one can retrieve solutions which have enough kinetic energy to become transonic at distances of few $\times 100r_g$. A subset amongst these solutions admit shock transitions when shock conditions are satisfied. This is the physical reason why some disk models show shock transitions and others do not (Lu *et al.* 1999; Das *et al.* 2009). Whether a flow will follow an ADAF solution or some kind of hybrid solution with or without shock will depend on the outer boundary condition and the physical processes dominant in the disc.

The shock model was later used to explain observations.

Chakrabarti & Titarchuk (1995); Chakrabarti & Mandal (2006); Mandal & Chakrabarti (2008, 2010) showed that the post-shock region being hotter, can produce the hard power-law tail by inverse-Comptonizing soft photons from pre-shock and post-shock parts of the accretion disc. The soft state and hard states are automatically explained depending on the existence or non-existence of the shock. Presence of such transonic advective flow has also been suggested by observations (Smith *et al.* 2001, 2002). Infact the ‘hardness-intensity-diagram’, or HID a hysteresis like behaviour seen in microquasars has been reproduced by this model (Mandal & Chakrabarti 2010). In other words, the post-shock region is the elusive Compton cloud.

Interestingly enough, the shock fronts are stable in a limited region of energy-angular momentum parameter space and naturally give rise to time dependent solutions whenever the exact momentum balance across the shock front is not achieved. This might be due to different rates of cooling (Molteni *et al.* 1996b), or different rates of viscous transport (Lanzafame *et al.* 1998; Lee *et al.* 2011). These oscillations were also confirmed by pure general relativistic simulations (Aoki *et al.* 2004; Nagakura & Yamada 2008, 2009). Molteni *et al.* (1996b) suggested that if the post-shock region oscillates, then the hard radiation produced by the post-shock region would oscillate as well, and hence explain the QPO. Infact, the evolution of QPO frequencies during the outburst states of various microquasars like XTEJ1550-654, GRO 1655-40 etc were explained by this model (Chakrabarti *et al.* 2009) by assuming inward drift of the oscillating shock due to increased viscosity of the flow.

Another interesting consequence of accretion shock is that, it automatically explains the formation of outflows. The unbalanced pressure gradient force in the axial direction drives matter in the form of outflows and may be considered as the precursor of jets (Molteni *et al.* 1994; Chakrabarti 1999; Chattopadhyay & Das 2007; Das & Chattopadhyay 2008). These outflows can be accelerated by various accelerating mechanisms to relativistic terminal speeds (Chattopadhyay *et al.* 2004; Chattopadhyay 2005). If the shock conditions are properly considered, then the mass outflow should reduce the pressure of the post-shock region and hence the shock would move inward, which in turn, would modify the shock parameter space in presence of massloss (Singh & Chakrabarti 2012). Another model of non-fluid bipolar outflows have been enthusiastically pursued by Becker and his collaborators which involves Fermi acceleration of particles in isothermal shocks (Le & Becker 2005; Becker *et al.* 2008; Das *et al.* 2009). The advantage of shock in accretion model is that the presence or absence of shock, is good enough to broadly explain many varied aspects of black holes candidates such as spectral states, QPOs, jets and outflows etc and the correlation between these aspects (Chakrabarti *et al.* 2009). Such correlations are also reported in observations (Smith *et al.* 2001, 2002; Gallo *et al.* 2003).

There are other jet generation models too. Apart from ADIOS, magnetically driven outflows were also proposed by many authors (Blandford & Znajek 1977; Blandford & Payne 1982; Proga 2005; Hawley *et al.* 2007). These magnetic bipolar outflows may be powered by the extraction of rotation energy of the black hole in the form of Poynting flux. However, recent observations finds weak

or no correlation of black hole spin with the jet formation around microquasars and are conjectured to be similar for AGNs as well (Fender *et al.* 2010). Bipolar outflows may even be powered by centrifugal or magnetic effect, and has been shown that for low angular momentum even weak magnetic fields can produce equatorial inflow, bipolar outflow, polar funnel inflow and polar funnel outflow, and magnetic effect was identified as the main driver of such outflows. Interesting as it may be, however, its connection with spectral and radiative state of black hole candidates is not well explored. It is well known that the spectra of the black hole candidates extends to high energy domain (\sim few MeVs), and one of the ways to generate such high energy non-thermal spectra is by shock acceleration of electrons, and has been used to explain spectra from black hole candidates (Chakrabarti & Mandal 2006; Mandal & Chakrabarti 2008). Not only hydrodynamic calculations, even magneto-hydrodynamic investigations bears the possibility of shock in accretion (Nishikawa *et al.* 2005; Takahashi *et al.* 2006). Therefore we are looking for solutions of outflow generation which incorporates shocks, although presently investigating the effect of viscosity in formation of such outflows.

Various simulations with Paczyński-Wiita potential (Molteni *et al.* 1994, 1996b,a; Lanzafame *et al.* 1998, 2008), as well as GRMHD simulations (Nishikawa *et al.* 2005) showed the presence of post-shock bipolar outflows, which are far from isothermal approximation. Therefore, presently we relax the strict isothermality condition, and concentrate on conservation of fluxes across the shock front. Theoretical frame work of thermally driven outflows has been done either for inviscid discs (Chakrabarti 1999; Das *et al.* 2001; Singh & Chakrabarti 2012), or for viscous discs where the viscous stress was assumed to be proportional to the total pressure (Chattopadhyay & Das 2007; Das & Chattopadhyay 2008). No theoretical investigations has thus far been made to study thermally driven outflows from discs where the viscous stress is proportional to the shear, a form of viscosity which is probably more realistic for black hole system (Becker & Subramaniam 2005). In this paper we solve viscous accretion disc equations for the contentious viscosity prescription, to compute the solution topologies of thermally driven outflows and the mass-outflow rates. We compute the energy angular-momentum parameter space for the accretion flows which will produce such outflows, and its dependence on viscosity parameter. In numerical simulation with Shakura & Sunyaev viscosity prescription, shock location seems to increase with the increase of viscosity parameter (Lanzafame *et al.* 1998; Lee *et al.* 2011), while theoretical investigations with Chakrabarti-Molteni viscosity prescription showed the opposite phenomenon (Chattopadhyay & Das 2007; Das & Chattopadhyay 2008). We address this issue and attempt to remove any ambiguity. Since the post-shock disc could well be the elusive Compton cloud, while the Shakura-Sunyaev viscosity might be more physical since it satisfies proper inner boundary conditions around black holes (Becker & Le 2003), studies of shock driven outflows and its dependence on viscosity would throw light in understanding the radio X-ray correlation from X-ray binaries, especially, whether the jet becomes stronger or weaker with the increasing viscosity parameter, this would have an interesting connotation in interpreting observations. Since the post-shock disc can produce high energy photons,

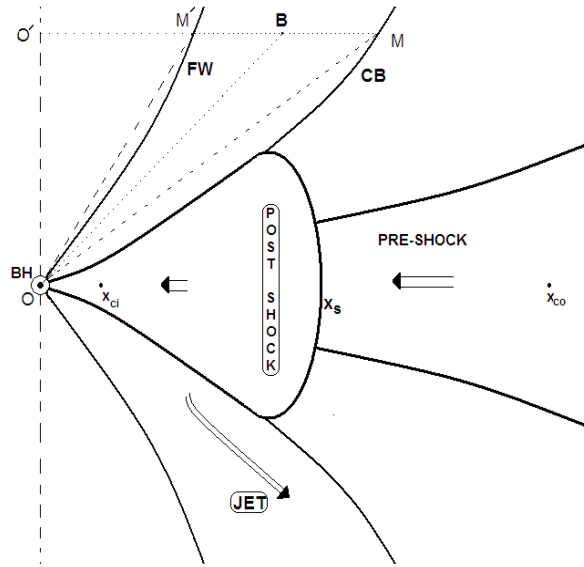


Figure 1. Schematic diagram of accretion-ejection flow geometry. The black hole (BH) with its horizon is shown at O . OO' is the z axis. $r_{CB} = OM$ and $r_{FW} = OM'$ are spherical radial distances of the Centrifugal Barrier (CB) and Funnel Wall (FW). Moreover, $x_{FW} = O'M'$, $x_{CB} = O'M$ are indicated. The two physical critical points x_{ci} and x_{co} of the accretion disc, and the shock location x_s is also shown. The jet flows through CB and FW.

then some part of the thermal energy gained through shocks will be dissipated as radiations. We study the issue of origin of such outflows in presence of dissipative shocks too.

In the next section, we present the simplifying assumptions and equations of motion. In section 3, we present the methodology of solution. In section 4, we present the solutions, and in the last section we present discussion and concluding remarks.

2 MODEL ASSUMPTIONS AND EQUATIONS OF MOTION

It has recently been stressed that black hole rotation plays no, or little part in generating or powering these jets (Fender *et al.* 2010). So it is expected that plasma processes or fluid properties of the disc would generate jets. In this paper, we consider a non-rotating black hole and focus only on the fluid properties of accretion disc, which may be considered to be responsible for jet generation. We have assumed the axis-symmetric disc-jet system to be in steady state. The space-time properties around a Schwarzschild black hole is described by the pseudo-Newtonian potential introduced by Paczyński & Wiita (1980). The viscosity prescription in the disc is described by the Shakura-Sunyaev prescription. We ignore any cooling mechanism in order to focus on the effect of viscosity. The jets are tenuous and should have less differential rotation than the accretion disc, as a result the viscosity in jets can be ignored. To negate any resulting torque, the angular momentum at the jet base is assumed same as that of the local value of angular momentum of the disc. The accretion disc occupies the space on or about the equatorial

plane. But the jet flow geometry is described about the axis of symmetry. We first present the equations of motions of the accretion disc and the jet separately in the subsequent part of this section, and then in the next section, we describe the method to obtain the self consistent accretion-ejection solution. In this paper we have used the geometric unit system where, $2G = M = c = 1$ (M is the mass of the black hole, G is the Gravitational constant). Therefore, in this representation the units of length, mass and time are the Schwarzschild radius or $r_g = 2GM/c^2$, M , and $r_g/c = 2GM/c^3$, respectively, consequently the unit of speed is c .

2.1 Equations of motion for accretion

The equations of motion for viscous accreting matter around the equatorial plane, in cylindrical coordinates (x, ϕ, z) are given by, the radial momentum equation:

$$u \frac{du}{dx} + \frac{1}{\rho} \frac{dp}{dx} + \frac{1}{2(x-1)^2} - \frac{\lambda^2(x)}{x^3} = 0 \quad (1)$$

The mass-accretion rate equation:

$$\dot{M} = 2\pi\Sigma ux, \quad (2)$$

The mass accretion rate \dot{M} is a constant of motion, except at the regions from where the mass may be lost into the jets. We present the exact form of the conservation of \dot{M} later in the paper. The angular momentum distribution equation:

$$u \frac{d\lambda(x)}{dx} + \frac{1}{\Sigma x} \frac{d(x^2 W_{x\phi})}{dx} = 0 \quad (3)$$

The entropy generation equation:

$$\Sigma u T \frac{ds}{dx} = Q^+ - Q^-. \quad (4)$$

The local variables u , a , p , ρ and λ in the above equations are the radial bulk velocity, sound speed, isotropic pressure and specific angular momentum of the flow, respectively. Here, $\Sigma = 2\rho h$ and $W_{x\phi}$ are the vertically integrated density and the viscous stress tensor (Matsumoto *et al.* 1984). Other quantities like the the entropy density, the local temperature, and the local half height of the disc are given by s , T , and h , respectively. The local heat gained and lost by the flow are given by $Q^+ = W_{x\phi}^2/(\eta)$ and Q^- .

The constant of motion of the flow is obtained, by integrating equation (1) with the help of equations (2 — 4), we find that the energy per unit mass is given by

$$E = \frac{u^2}{2} + \frac{a^2}{\gamma - 1} - \frac{\lambda^2}{2x^2} + \frac{\lambda_0 \lambda}{x^2} + \Phi(x), \quad (5)$$

and is also called as the specific grand energy of the flow, and is conserved throughout the flow even in the presence of viscous dissipation (Gu & Lu 2004), except across a dissipative shock (see, section 3.1.1). In Eq. (5), $\Phi(x) = -0.5/(x-1)$ is the pseudo-Newtonian gravitational potential.

The viscous stress is given by

$$W_{x\phi} = \eta x \frac{d\Omega}{dx}, \quad (6)$$

where, $\eta = \rho\nu h$ is the dynamic viscosity coefficient, $\nu = \alpha^2/(\gamma\Omega_k)$ is the kinematic viscosity, α is the Shakura-Sunyaev viscosity parameter, Ω and Ω_k are the local angular velocity and local Keplerian angular velocity, respectively.

Considering hydrostatic equilibrium in vertical direction, the local disc half height is obtained as:

$$h(x) = \sqrt{\frac{2}{\gamma}} a x^{1/2} (x-1) \quad (7)$$

The adiabatic sound speed is defined as

$$a = \sqrt{\frac{\gamma p}{\rho}} \quad (8)$$

where γ is adiabatic index. The expression of the entropy-accretion rate is given by,

$$\dot{\mathcal{M}}(x) = \frac{a^{(2n+1)} u x}{\Omega_k}, \quad (9)$$

If there is no viscosity *i.e.*, $\alpha = 0$, then $\dot{\mathcal{M}}$ is constant except at the shock. At shock the entropy accretion rate will suffer discontinuous jump. The immediate pre-shock and post shock entropy-accretion rate denoted as $\dot{\mathcal{M}}_-$ and $\dot{\mathcal{M}}_+$, are related as $\dot{\mathcal{M}}_+ > \dot{\mathcal{M}}_-$. But for $0 < \alpha < 1$ or viscous flow, $\dot{\mathcal{M}}$ varies continuously in the disc since viscosity dissipates and increases the entropy. If shock exists in viscous flow then, similar to the inviscid case $\dot{\mathcal{M}}_+ > \dot{\mathcal{M}}_-$.

The gradient of the angular velocity can be obtained by integrating equation (3) and also by utilizing equation (2) and the expression of $W_{x\phi}$,

$$\frac{d\Omega}{dx} = -\frac{\gamma u \Omega_k (\lambda - \lambda_0)}{\alpha a^2 x^2}. \quad (10)$$

where, λ_0 is specific angular momentum at the horizon obtained by considering vanishing torque at the event horizon (Weinberg 1972; Becker *et al.* 2008). Since $\lambda = x^2 \Omega$, the radial derivative of λ is given by

$$\frac{d\lambda}{dx} = 2x\Omega + x^2 \frac{d\Omega}{dx}. \quad (11)$$

Moreover, Ω_k denotes the Keplerian angular velocity and defined as

$$\Omega_k^2(x) = \frac{1}{2x(x-1)^2}, \quad (12)$$

The Keplerian specific angular momentum is defined as

$$\lambda_k = \Omega_k x^2 = \left[\frac{x^3}{2(x-1)^2} \right]^{1/2}. \quad (13)$$

Manipulating equations (1 — 4), with the help of equations(7 — 13) we obtain,

$$\frac{du}{dx} = \frac{N}{D}. \quad (14)$$

where,

$$N = \frac{2}{\gamma+1} \frac{(5x-3)u}{2x(x-1)} + \frac{(\lambda^2 - \lambda_k^2)u}{a^2 x^3} + \gamma^2 \left(\frac{\gamma-1}{\gamma+1} \right) \frac{u^2 \lambda_k (\lambda - \lambda_0)^2}{\alpha a^4 x^4}$$

and

$$D = \frac{u^2}{a^2} - \frac{2}{\gamma+1}$$

The gradient of the sound speed is,

$$\frac{da}{dx} = \left(\frac{a}{u} - \frac{\gamma u}{a} \right) \frac{du}{dx} + \frac{(5x-3)a}{2x(x-1)} + \frac{\gamma(\lambda^2 - \lambda_k^2)}{a x^3}. \quad (15)$$

Therefore, the accretion disc problem in vertical equilibrium is solved by integrating Eqs. (11, 14, 15).

2.1.1 Critical point conditions for accretion

At large distances away from the horizon the inward velocity is very small and therefore the flow is subsonic, but, matter enters the black hole with the speed of light and therefore it is supersonic close to the horizon. Hence accreting matter around black holes must be transonic, since it makes a transition from subsonic to supersonic. Therefore, at some location the denominator D of Eq. (14), will go to zero, and hence the numerator N goes to zero too. Such a location is called the sonic point or critical point. The critical point conditions are given as:

$$M_c^2 = \frac{u_c^2}{a_c^2} = \frac{2}{\gamma + 1} \quad (16)$$

$$\left[\frac{(5x_c - 3)M_c^2}{2x_c(x_c - 1)} \right] a_c^3 + \left[\frac{(\lambda_c^2 - \lambda_k^2)}{x_c^3} \right] a_c + \gamma^2 \left(\frac{\gamma - 1}{\gamma + 1} \right) \frac{M_c \lambda_k (\lambda_c - \lambda_0)^2}{\alpha x_c^4} = 0 \quad (17)$$

where M_c , u_c , a_c , x_c and λ_c are Mach number, the bulk velocity, the sound speed, the radial distance and the specific angular momentum at the critical point, respectively.

The radial velocity gradient at the critical point is calculated by employing the l'Hospital rule.

$$\left(\frac{du}{dx} \right)_c = \left(\frac{dN/dx}{dD/dx} \right)_{r=r_c} \quad (18)$$

and by combining Eqs. (15 & 18) we get,

$$\left(\frac{da}{dx} \right)_c = \left(\frac{a_c}{u_c} - \frac{\gamma u_c}{a_c} \right) \left(\frac{du}{dx} \right)_c + \frac{(5x_c - 3)a_c}{2x_c(x_c - 1)} + \frac{\gamma(\lambda_c^2 - \lambda_{kc}^2)}{a_c x_c^3}. \quad (19)$$

So, the solution of Eqs. (11, 14, 15), can only be obtained if we know the sonic point and its conditions (Eqs. 16–19).

2.2 Equations of motion for outflows

The flow geometry for accretion is described about the equatorial plane, however, the jet or outflow geometry is about the axis of symmetry. If the outflow posses some angular momentum, then the outflow geometry should be hollow. Indeed, numerical simulations by Molteni *et al.* (1996a) suggests that the outflowing matter tends to emerge out between two surfaces namely, the funnel wall(FW) and centrifugal barrier(CB). In Fig.1, the schematic diagram of the jet geometry is shown. The centrifugal barrier(CB) surface is defined as the pressure maxima surface and is expressed as

$$x_{CB} = [2\lambda^2 r_{CB}(r_{CB} - 1)]^{\frac{1}{4}} \quad (20)$$

where, $r_{CB} = \sqrt{x_{CB}^2 + y_{CB}^2}$, spherical radius of CB. Here, x_{CB} and y_{CB} are the cylindrical radius and axial coordinate (i.e., height at r_{CB}) of CB. We compute the jet geometry with respect to y_{CB} i.e., $y_{FW} = y_j = y_{CB}$, where y_{FW} and y_j are the height of FW and the jet at r_{CB} , respectively. The FW is obtained by considering null effective potential and is given by

$$x_{FW}^2 = \lambda^2 \frac{(\lambda^2 - 2) + \sqrt{(\lambda^2 - 2) - 4(1 - y_{CB}^2)}}{2} \quad (21)$$

where, x_{FW} is the cylindrical radius of FW. We define the cylindrical radius of the outflow

$$x_j = \frac{x_{FW} + x_{CB}}{2} \quad (22)$$

The spherical radius of the jet is given by $r_j = \sqrt{x_j^2 + y_j^2}$. In Fig.1, OB(= r_j) defines the streamline (solid) of the outflow. The total area function of the jet is defined as,

$$\mathcal{A} = \frac{2\pi(x_{CB}^2 - x_{FW}^2)}{\sqrt{1 + (dx_j/dy_j)^2}}, \quad (23)$$

where, the denominator is the projection effect of the jet streamline on its cross-section. The integrated radial momentum equation for jet is given by,

$$\mathcal{E}_j = \frac{1}{2}v_j^2 + na_j^2 + \frac{\lambda_j^2}{2x_j^2} - \frac{1}{2(r_j - 1)} \quad (24)$$

where, \mathcal{E}_j is the specific energy, λ_j is the angular momentum of the jet, and $n = 1/(\gamma - 1)$ is the polytropic index. The integrated continuity equation is,

$$\dot{M}_{out} = \rho_j v_j \mathcal{A} \quad (25)$$

and the entropy generation equation is integrated to obtain the polytropic equation ($p_j = K_j \rho_j^\gamma$) of state for the jet. The entropy accretion rate for the jet is given by

$$\dot{\mathcal{M}}_j = a_j^{2n} v_j \mathcal{A} \quad (26)$$

In Eqs. (24-25), the suffix 'j' indicates jet variables, where v_j , a_j , and ρ_j are the velocity, the sound speed and the density of the jet.

Equations (24-25) are differentiated with respect to $r(= r_{CB})$, to obtain,

$$\frac{dv_j}{dr} = \frac{\mathcal{N}}{\mathcal{D}}, \quad (27)$$

where,

$$\mathcal{N} = \frac{1}{2(r_j - 1)^2} \frac{dr_j}{dr} - \frac{\lambda_j^2}{x_j^3} \frac{dx_j}{dr} - \frac{a_j^2}{\mathcal{A}} \frac{d\mathcal{A}}{dr}, \quad (28)$$

and,

$$\mathcal{D} = \frac{a_j^2}{v_j} - v_j. \quad (29)$$

The critical point(r_{jc}) condition for jet is,

$$v_{jc}^2 = a_{jc}^2 = \left[\frac{1}{2(r_{jc} - 1)^2} \left(\frac{dr_j}{dr} \right)_{r_c} - \frac{\lambda_{jc}^2}{x_{jc}^3} \left(\frac{dx_j}{dr} \right)_{r_c} \right] \left[\frac{1}{\mathcal{A}_c} \left(\frac{d\mathcal{A}}{dr} \right)_{r_c} \right]^{-1}. \quad (30)$$

The outflow solution is obtained by integrating Eqs. (27), with the help of Eq. (30). The outflow equations can be determined uniquely if \mathcal{E}_j and λ_j are known, because, the value of \mathcal{E}_j and λ_j determines r_{jc} . However, for consistent accretion-ejection solution, both accretion and jet part have to be solved simultaneously, a technique previously used by Chattopadhyay & Das (2007), and has been refined in this paper.

3 METHODOLOGY

The accretion-ejection solutions are self consistently and simultaneously solved, and we present the methodology to

find such solutions in this section. We start with the solution of the accretion disc. It has been mentioned before that Eqs. (11, 14, 15) can be integrated, if we know the sonic point x_c . One of the long standing problem in accretion physics is to determine the sonic point of the flow in presence of a viscous stress of the form Eq. (6), which keeps the angular momentum equation in a differential form [Eq. (11)] rather than an algebraic form (Chakrabarti 1996; Gu & Lu 2004). The problem is compounded by the fact that although quantities on the horizon are known, but the coordinate singularity on the horizon makes it difficult to solve the equations by taking those as the starting values. The problem could be circumvented if the asymptotic values of the flow variables are known close to the horizon.

With a clever use of conservation equations Becker & Le (2003) found the asymptotic distribution of the specific angular momentum and the radial velocity close to the horizon, and they are,

$$\lambda(x) = \lambda_0 \left[1 + \frac{2\alpha}{\gamma r_g} \left(\frac{2}{r_g} \right)^{1/2} \left(\frac{\dot{M}^2}{2r_g^3} \right)^{\frac{\gamma-1}{\gamma+1}} (x-r_g)^{\frac{\gamma+5}{2\gamma+2}} \right], \quad x \rightarrow 1 \quad (31)$$

and

$$u(x) = u_{ff}(x) \left[1 + \frac{2Ex^2 - \lambda_0^2 - (\gamma+1)f(x)}{x^2 u_{ff}^2(x) - (\gamma-1)f(x)} \right]^{1/2}, \quad x \rightarrow 1 \quad (32)$$

where the function $f(x)$ is $f(x) = \frac{2x^2}{\gamma^2 - 1} \left[\frac{\dot{M}^2}{2x^3(x-r_g)} \right]^{\frac{\gamma-1}{\gamma+1}}$ and the free fall velocity in the pseudo-Newtonian potential geometry is given by

$$u_{ff}(x) = \frac{1}{\sqrt{(x-1)}} \quad (33)$$

3.1 Integration procedure of accretion solution

A position very close to the horizon $x = x_{in} = 1.01$ is chosen. For given values of the parameters α , E , λ_0 at the horizon and \dot{M}_{in} at x_{in} , Eqs. (31), (32) and (33) can be used to determine the asymptotic values of the fluid variables close to the horizon, and which can be used as the initial values for the integration. With these values, Eqs. (11, 14, 15) are integrated outwards, simultaneously checking for the location of the sonic point by using Eqs. (16–19). The sonic point x_c is determined iteratively, and once it is found, the sonic point conditions are used to integrate the equations of motions, outwards. It is well known that matter with angular momentum may possess *multiple critical points* (MCP). But the flow may pass through various sonic points only if a shock is present, in other words, the existence of MCP is mandatory for the formation of shock in black-hole accretion. Only a supersonic flow can undergo shock transition and so existence of one sonic point at larger distance (*i.e.*, x_{co}) from the horizon is warranted. The post shock flow is subsonic. However, the inner boundary condition of black hole accretion is supersonic, and hence the subsonic post-shock flow has to pass through another sonic point (x_{ci}), before it dives into the black hole. In other words, shock in black hole accretion may exist only if MCP exists. It is to be remembered though, that there is no smooth transition between various branches

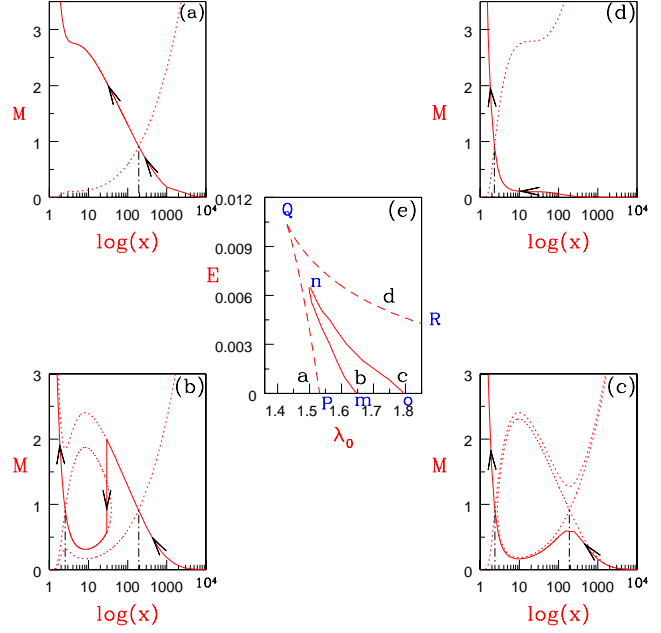


Figure 2. The domain for multiple critical point MCP (dashed) and shock (solid) in $E - \lambda$ parameter space (e) is presented. The solution topologies or the plot of Mach number M with $\log(x)$ of the O type for $E = 0.001$, $\lambda = 1.5$ (a); A type for $E = 0.001$, $\lambda = 1.68$ (b); W type for $E = 0.001$, $\lambda = 1.75$ (c); and I type for $E = 0.005$, $\lambda = 1.77$ (d), are presented. The solution type and their location in the parameter space is also indicated in (e). All the plots are for $\alpha = 0$. The dotted lines in the panels named a, b, c, and d show all possible solutions while, the solid line with arrow heads show the actual accretion solution. The vertical long-short dashed line shows the location of the sonic points.

of the solution passing through different sonic points. This is true for both inviscid and adiabatic flows as well as viscous and non-adiabatic flow. However, if the flow is inviscid, for a given value of E and λ_0 all possible sonic points are known a priori. In case of viscous flow which is following a viscosity prescription of the form Eq. (6), the existence of multiple sonic points can only be ascertained only if there is a shock.

3.1.1 Shock equations

The Rankine Hugoniot (RH) shock conditions are obtained by conservation of the mass, momentum and energy flux across the shock. In presence of mass loss and energy loss, the shock conditions are given by, the modified mass conservation,

$$\dot{M}_+ = \dot{M}_- - \dot{M}_{out} = \dot{M}_- (1 - R_{in}), \quad (34)$$

This equation effectively divides the accretion rate of pre-shock accretion disc (\dot{M}_-) into two channels, namely the post-shock accretion disc (represented by \dot{M}_+) and the jet (represented by \dot{M}_{out}). The modified momentum conservation,

$$W_+ + \Sigma_+ u_+^2 = W_- + \Sigma_- u_-^2, \quad (35)$$

and the third shock condition is the modified energy conservation

$$E_+ = E_- - \Delta E, \quad (36)$$

where, $R_{\dot{m}}$ is the relative mass outflow rate given by,

$$R_{\dot{m}} = \frac{\dot{M}_{out}}{\dot{M}_-}. \quad (37)$$

Here, subscripts minus(-) and plus(+) denote the quantities before and after the shock. W is the vertically integrated pressure. In absence of massloss ($R_{\dot{m}} = 0$) or dissipation (*i.e.*, $\Delta E = 0$), Eqs. (34, 35, 36) reduce to the standard RH shock conditions. Since the dissipation is expected at the shock location, it is assumed that energy dissipation takes place mostly through the thermal Comptonization (Chakrabarti & Titarchuk 1995; Mandal & Chakrabarti 2010) and is likely to be very important within a distance dx inside the shock where the optical depth is around unity. So this energy dissipation in the post shock flow reduces the temperature of the flow and the loss of energy is proportional to the temperature difference between the post-shock and the pre-shock flows, *i.e.*

$$\Delta E = f_e n (a_+^2 - a_-^2). \quad (38)$$

where f_e is the fraction of the difference in thermal energy dissipation across the shock transition and n is the polytropic index. We use f_e as a parameter, in presence of detailed radiative processes f_e can be self-consistently determined. Since shock width is infinitesimally thin, so we assume that $d\Omega/dx$ is continuous across the shock. The angular momentum jump condition is calculated by considering the conservation of angular momentum flux, and is given by

$$\lambda_- = \lambda_+ + C_{sh} \left[\frac{a_+^2}{u_+} - \frac{a_-^2}{u_-} \right], \quad (39)$$

where, $C_{sh} = -u_+(\lambda_+ - \lambda_0)/a_+^2$. Equation (39) can be re-written as,

$$(\lambda_- - \lambda_0) = \frac{a_-^2 u_+(\lambda_+ - \lambda_0)}{a_+^2 u_-} \quad (40)$$

Since at shock, $a_+ > a_-$ and $u_- > u_+$, therefore, $\lambda_+ > \lambda_-$.

Using shock condition equations (34) and (35), the pre-shock sound speed and bulk velocity can be written as,

$$a_-^2 = k_1 u_- - \gamma u_-^2 \quad (41)$$

where, $k_1 = (a_+^2 + \gamma u_+^2)/(f u_+)$, $f = 1/(1 - R_{\dot{m}})$. Now substituting for a_- and λ_- in equation (36), we find a quadratic equation of u_- as,

$$C_2 u_-^2 + C_1 u_- + C_0 = 0 \quad (42)$$

where,

$$C_2 = \left[\frac{1}{2} - n\gamma(1 + f_e) - \frac{\gamma^2 C_{sh}^2}{2x_s^2} \right],$$

$$C_1 = \left[n(1 + f_e)k_1 - \frac{\gamma C C_{sh}}{x_s^2} + \frac{\gamma \lambda_0 C_{sh}}{x_s^2} \right],$$

$$C_0 = \left[\frac{\lambda_0 C}{x_s^2} - \frac{C^2}{2x_s^2} - k_2 \right],$$

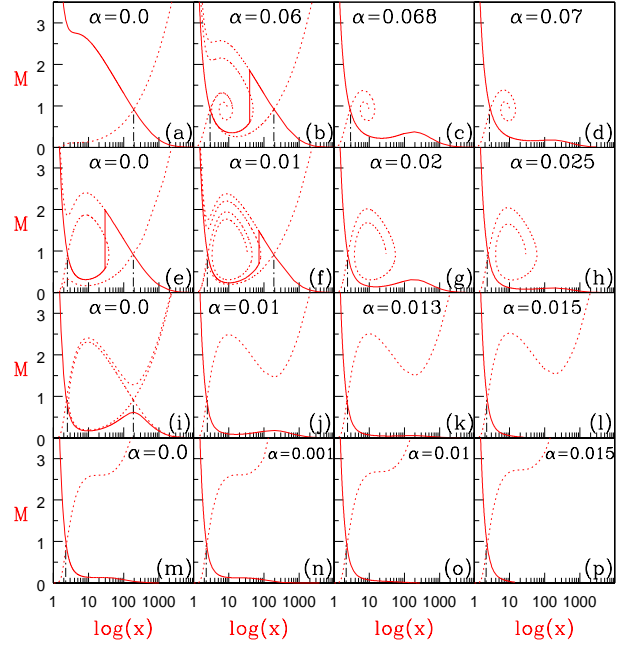


Figure 3. Variation of M with $\log(x)$ for the accretion solutions with different viscosity parameter α . In a, e, i, m we present inviscid solutions corresponding to the O, A, W, I type of solutions from Figs. 2a-d. Towards right E , λ_0 is kept the same but α is increased. The flow parameters for which these plots are generated $E = 0.001$, $\lambda = 1.5$ (a, b, c, d); $E = 0.001$, $\lambda = 1.68$ (e, f, g, h); $E = 0.001$, $\lambda = 1.75$ (i, j, k, l) and $E = 0.005$, $\lambda = 1.75$ (m, n, o, p). The viscosity parameter α is mentioned on the figure. The vertical long-short dashed line shows the location of sonic points.

$$C = \lambda_+ + C_{sh} \left[\frac{a_+^2}{u_+} - k_1 \right]$$

and

$$k_2 = E_+ - \Phi(x_s) + f_e n a_+^2.$$

In terms of the shock quantities, the mass outflow rate is given by

$$R_{\dot{m}} = \dot{M}_{out}/\dot{M}_- = \frac{R v_j(x_s) \mathcal{A}(x_s)}{4\pi \sqrt{\frac{2}{\gamma}} x_s^{3/2} (x_s - 1) a_+ u_-} = RV\mathcal{G}, \quad (43)$$

where, $R = \Sigma_+/\Sigma_-$ is the compression ratio across the shock, $\mathcal{V} = v_j(x_s)/u_-$ is the ratio of jet base velocity and the pre-shock velocity of the disc (u_-), and $\mathcal{G} = \mathcal{A}(x_s)/[4\pi(2/\gamma)^{1/2} x_s^{3/2} (x_s - 1) a_+]$ is the ratio of the jet cross-sectional area at $r = x_s$ and the post-shock accretion disc cross-sectional area.

3.2 Accretion-Ejection Solution

The accretion-ejection is computed self-consistently. We have set $\gamma = 1.4$ and $x_{in} = 1.01$ throughout the paper. The method to find the accretion-ejection solution is as follows,

(i) First we assume that $R_{\dot{m}} = 0$. With chosen values of λ_0 , E , α and f_e , we follow the procedure described in section 3.1, *i.e.*, determine the inner sonic point iteratively and integrate outwards. Equations (39, 41, 42) are checked

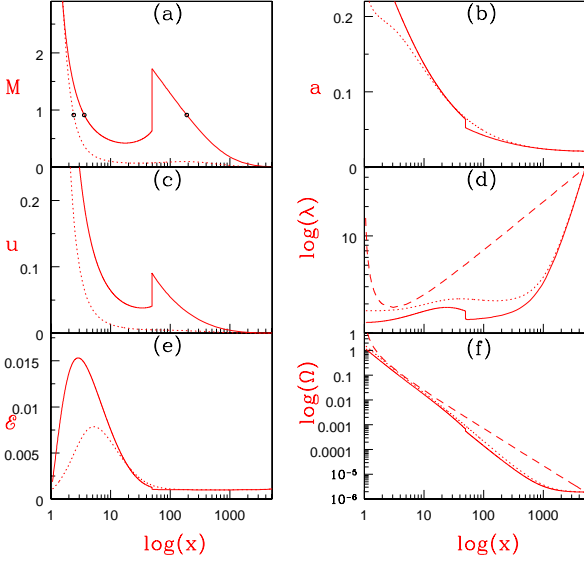


Figure 4. Comparison of shock free (dotted) and shocked solution (solid). Both the solution starts with the same outer boundary condition $x_{inj} = 5117$, $\lambda_{inj} = \lambda_K(x_{inj}) = 50.6$, $E = 10^{-3}$. The viscosity parameter for the shock free solution is $\alpha = 0.02$ (dotted) and that for the shocked one $\alpha = 0.15$ (solid). Various flow variables are plotted are M (a), a (b), u (c), λ (d), \mathcal{E} (e) and Ω (f) as a function of x . The sonic points are marked with open circles (a). The shock free solution has only one x_{ci} , the shocked solution has both x_{ci} and x_{co} and the shock location is at $x_s = 49.68$. Dashed plots of λ_K and Ω_K in (d) and (f) are Keplerian angular momentum and angular velocity drawn for comparison.

to calculate the pre-shock quantities. We find out the outer sonic point (x_{co}) iteratively, from the pre-shock quantities. Two possibilities may arise, either the flow passes through only one sonic point and gives a smooth solution, or, finds a stable shock solution and passed through two sonic points. The location of the jump for which x_{co} exists is the virtual shock location (\tilde{x}_s).

(ii) Once \tilde{x}_s is found out, we assign $\mathcal{E}_j = \mathcal{E}_+$ and $\lambda_j = \lambda_+$ and solve jet Eqs. (27 & 30) and compute the corresponding R_{in} .

(iii) We put this value of R_{in} into Eqs. (39-42) to find a new shock location .

(iv) Steps (ii) & (iii) are repeated till the temporary shock location \tilde{x}_s converges to the actual shock location (x_s). The converged shock solution therefore gives the actual jet solution too. We find that the $\dot{M}_j > \dot{M}_-$ and $\dot{M}_+ > \dot{M}_-$. Since matter prefers higher entropy solutions, therefore, the post-shock fluid would prefer both the channels, one through the x_{ci} onto the black hole, and the other through r_{jc} and out of the disc-jet system. In other words, a shock in accretion would generate a bipolar outflow from the post-shock region too.

The outer boundary is chosen as $x_{inj} = 10^4 r_g$, or the distance at which $\lambda(x_{inj}) = \lambda_K(x_{inj})$, which ever is shorter.

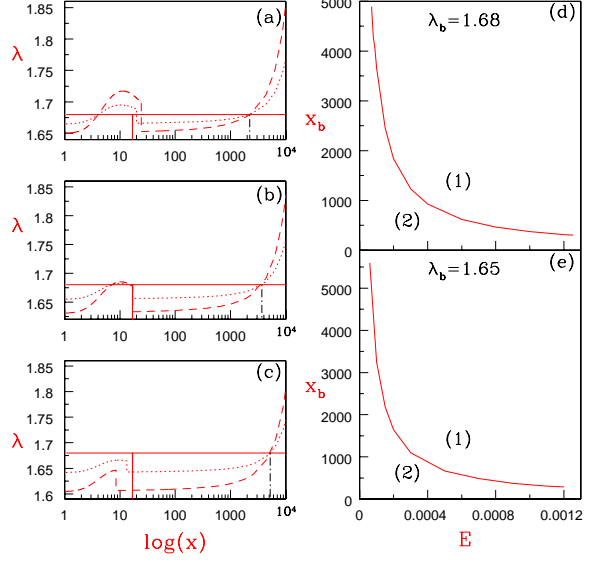


Figure 5. Variation of λ with $\log(x)$ of shocked accretion flow (a, b, c), for parameters $E = 0.0001$, & $\lambda_b = 1.68$. Each curve represents $\alpha = 0.0$ (solid), $\alpha = 0.0075$ (dotted) and $\alpha = 0.015$ (dashed). First three panels are for $x_b = 2220 r_g$ (a), $x_b = 3660 r_g$ (b), and $x_b = 5230 r_g$ (c). Vertical solid line and dash-dotted line show the shock location for $\alpha = 0.0$ curve and outer boundary location (x_b), respectively. The variation of limiting x_b with E for $\lambda_b = 1.68$ (d), and $\lambda_b = 1.65$ (e). Domain 1 represents all x_b for which x_s decrease with the increase with α , but for any x_b in 2, x_s will increase with the increase of α .

4 SOLUTIONS

We present every possible way matter can dive into the black hole. In this section, we start with accretion solutions without considering massloss or dissipation at the shock front and study the effect of viscosity on accretion solution. Then we present the accretion-ejection solution and study how the viscosity can affect the mass outflow rates. And finally we present accretion-ejection solutions in presence of dissipative shocks and show the effect of both the viscosity and dissipation at the shock front.

4.1 All possible accretion solutions in the advective regime

Since black hole accretion is necessarily transonic, at first, we present the simplest rotating transonic solutions *i.e.*, inviscid global solutions (global solution \equiv which connect horizon and large distances) in Figs. 2a-d. The inviscid solutions are presented as an attempt to recall the simplest accretion case (Chakrabarti 1989; Das *et al.* 2001). For inviscid flow the constants of motions are E , λ ($= \lambda_0$), and if outflows are not present then, \dot{M} is also a constant of motion. Moreover, in absence of viscosity, it straightaway follows from Eq. (5) that $E = \mathcal{E} = u^2/2 + na^2 + \lambda^2/(2x^2) - 0.5/(x-1)$, where \mathcal{E} is the Bernoulli parameter or the specific energy of the flow. In Figs. 2a-d, accretion solutions in terms of the Mach number M ($= u/a$) distribution are presented, and in Fig. 2e, the $E - \lambda_0$ parameter space for multiple sonic point and the

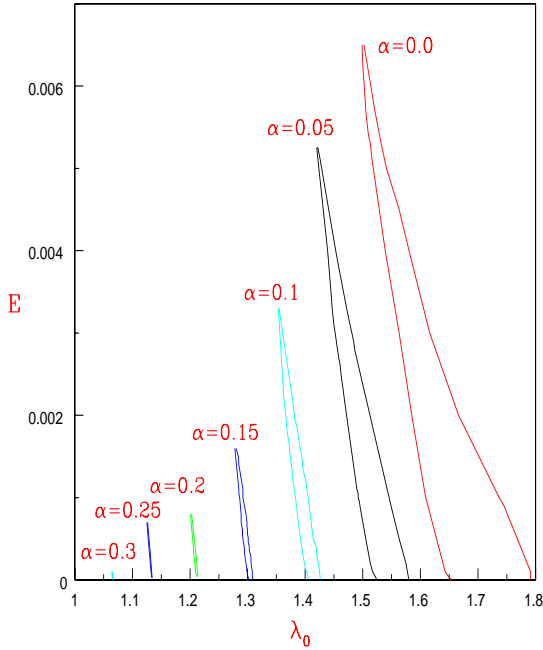


Figure 6. E — λ_0 parameter space for shock, for various viscosity parameters $\alpha = 0, 0.05, 0.1, 0.15, 0.2, 0.25, 0.3$ marked on the figure. No energy dissipation ($f_e = 0.0$) at the shock and no mass loss ($f = 1.0$) is assumed.

shock is presented too. Depending on E & λ_0 of the flow, the solutions are also different. If the λ_0 is low, there is only one outer sonic point x_{co} , and solution type is O-type or Bondi type ($E = 0.001$, $\lambda_0 = 1.5$, Fig. 2a). As λ_0 is increased, the number of physical sonic points increases to two and the accretion flow which becomes supersonic through x_{co} can enter the black hole through x_{ci} if a shock condition is satisfied. Although the shock free solution is possible but in this part of the parameter space a shocked solution will be preferred because a shocked solution is of higher entropy (or in other words of higher \dot{M}). Such a class of solution is called A-type ($E = 0.001$, $\lambda_0 = 1.68$, Fig. 2b). For even higher λ_0 only one sonic point is possible ($E = 0.001$, $\lambda_0 = 1.75$ for Type W; and $E = 0.005$, $\lambda_0 = 1.77$ for I shown in Figs 2c and d), and the solutions are wholly subsonic till x_{ci} and then dives on to blackhole supersonically. W type solutions are different than I type, in the sense, W type is still within the MCP domain while I type is not. Moreover, I type is a smooth monotonic solution, although W is smooth and shock free but is not monotonic and has an extremum at around x_{co} . The parameter space $E - \lambda_0$, bounded by solid line (mno) shows the RH shock parameter space, while the dotted one (PQR) shows the MCP domain (Fig. 2e). It is to be noted, that in the inviscid limit, accretion is only possible if $\lambda_0 < \lambda_K$.

Figures 3a, 3e, 3i, 3m, represent the inviscid solutions corresponding to the O type solutions (E , $\lambda_0 = 0.001, 1.5$), A type (E , $\lambda_0 = 0.001, 1.68$), W-type (E , $\lambda_0 = 0.001, 1.8$), and I-type (E , $\lambda_0 = 0.006, 1.8$), and are also depicted in Figs. 2a-d. Keeping E & λ_0 same,

we increase the viscosity parameter in the right direction. Figures 3a-d, has same E & λ_0 , but progressively increasing $\alpha = 0.06$ (Fig. 3b), 0.068 (Fig. 3c) and 0.1 (Fig. 3d). Similarly for Figs. 3e-h, $E - \lambda_0$ is same but different α , so is the case for Figs. 3i-l, and Figs. 3m-p. Interestingly, the viscous I type is in principle the much vaunted ADAF type solution presented in Figs 3d, 3h, 3k-l, and 3n-p. The shock-free solution is characterized by monotonic spatial distribution of flow variables, and wholly subsonic except very close to the horizon which are essentially the viscous I type solutions and has also been shown by Lu *et al.* (1999); Becker *et al.* (2008); Das *et al.* (2009). It is evident from Figs. 3a-p, that the effect of viscosity is to create additional sonic points in some part of the parameter space, opening up of closed topologies, and might trigger shock formation where there was no shock, while removing both shock and multiple critical points in other regime of the parameter space. All of this is achieved by removing angular momentum outwards while increasing the entropy inwards. In this connection one may find two kind of critical viscosity parameters in the advective domain. If the inviscid solution is O type (Fig. 3a), then there would be a lower bound of critical viscosity α_{cl} which would transport angular momentum in a manner that would trigger the standing shock. And there would be another upper bound of viscosity parameter α_{cu} that would quench the standing shock. While, if the inviscid solution has a shock to start with (Fig. 3e), then there could only be α_{cu} . For the case presented in Figs. 3a-d, $\alpha_{cl} = 0.0465$ and $\alpha_{cu} = 0.065$. And for the case presented in Figs. 3e-h, $\alpha_{cu} = 0.0126$.

So far, we have compared solutions with different viscosity but same internal boundary condition (E , λ_0). Let us compare two solutions with same outer boundary condition. In Figs. 4a-e, we compare two solutions starting at the same outer boundary $x_{inj} = 5117$, same grand energy $E = 10^{-3}$ and $\lambda_{inj} = \lambda_K(x_{inj}) = 50.6$. Both the solution starts with the same entropy $\sim \dot{M}_{inj} = 2.72 \times 10^{-5}$. For $\alpha = 0.15$ (solid) the accretion solution has a standing shock at $x_s = 49.68$ (the vertical jump in solid), while the shock free solution is for $\alpha = 0.02$ (dotted). The flow variables plotted are M (Fig. 4a), a (Fig. 4b), u (Fig. 4c), λ (Fig. 4d), and \mathcal{E} (Fig. 4e). In case of inviscid flow $E = \mathcal{E}$ is constant, for viscous flow E is still a constant of motion but \mathcal{E} , the specific energy, varies with x as is shown in Fig. 4e. The inner part of the shocked solution is faster, hotter, and of lesser angular momentum. The inner boundary for the shocked flow is $E = 10^{-3}$, $\lambda_0 = 1.29$, while that for the shock free solution is $E = 10^{-3}$, $\lambda_0 = 1.7$. The jump in λ at the shock follows Eq. 40. Interestingly, the post shock flow is of higher entropy [$\dot{M}(x \sim 1) = 7.49 \times 10^{-5}$] than the inner part of the shock free solution [$\dot{M}(x \sim 1) = 7.12 \times 10^{-5}$]. Although it may seem contradictory that a shock free solution exists for lower α , while shocked solution appears for higher α , however, it is to be remembered that with such high λ_{inj} , there would be no accretion solution for $\alpha = 0$. One has to have a certain non-zero viscosity to even have a global (that connects horizon and outer edge) solution. Infact, for this particular case we have identified a limiting viscosity parameter $\alpha_1 = 0.00747$, such that advective global solutions are possible for any viscosity parameter $\alpha \geq \alpha_1$. And for flows starting with such high initial λ , if the viscosity parameter α is small, then the λ distribution will be

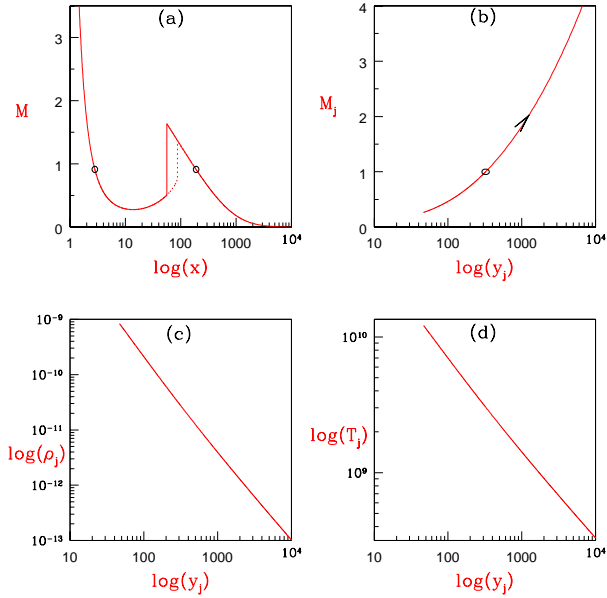


Figure 7. Mach number distribution for self-consistent accretion-ejection solution (a & b). The disc solution (a), and the jet (b) are plotted for accretion flow parameters $E = 0.001$, $\lambda_0 = 1.542$ and $\alpha = 0.05$. The shock in accretion is shown by the vertical jump at $x_s = 56.236$ (a). The density distribution ρ_j (c) and the temperature T_j distribution of the jets are also plotted (d). The sonic points are marked by open circles (a & b). The dotted vertical line shows the position of the shock if $R_m = 0$. The jet flow parameters $\mathcal{E}_j = \mathcal{E}_+ = 1.084 \times 10^{-3}$, $\lambda_j = \lambda_+ = 1.699$.

higher. Therefore, for such high λ radial velocities will not be high enough to become supersonic and form a shock. So one needs higher $\alpha \geq \alpha_{cl} = 0.1496$ to reduce the angular momentum to the extent that may produce standing accretion shock. And if α is increased beyond another critical value $\alpha_{cu} = 0.1555$, steady shock is not found. Hence one can identify three critical α 's for accretion flows starting with the same outer boundary condition, where the angular momentum at the outer boundary is local Keplerian value. Interestingly, α prescription originally invoked to generate Keplerian disc (Shakura & Sunyaev 1973), can produce sub-Keplerian accretion flow with or without shock even if angular momentum is Keplerian at the outer boundary. This is not surprising since, the gravitational energy released by the infalling matter, would be converted to kinetic energy and thermal energy (by compression and viscous dissipation). If the gravitational energy is converted to thermal energy and only the rotation part of kinetic energy, and also if the thermal energy gained by viscous dissipation is efficiently radiated away, then one would produce Keplerian disc solutions. The λ_K (Fig. 4d) and Ω_K (Fig. 4f) are presented for comparison. In the present paper, the radiative processes have been ignored which produces hot flow, but the advection terms have not been ignored. Therefore, sub-Keplerian flow with significant advection are obtained.

The effect of α on shock location x_s is an interesting issue. Numerical simulations show that, for fixed outer boundary condition, x_s expands to larger distances with the increase of α (Lanzafame *et al.* 1998; Lee *et al.* 2011), while analytically Chattopadhyay & Das (2007) showed that for

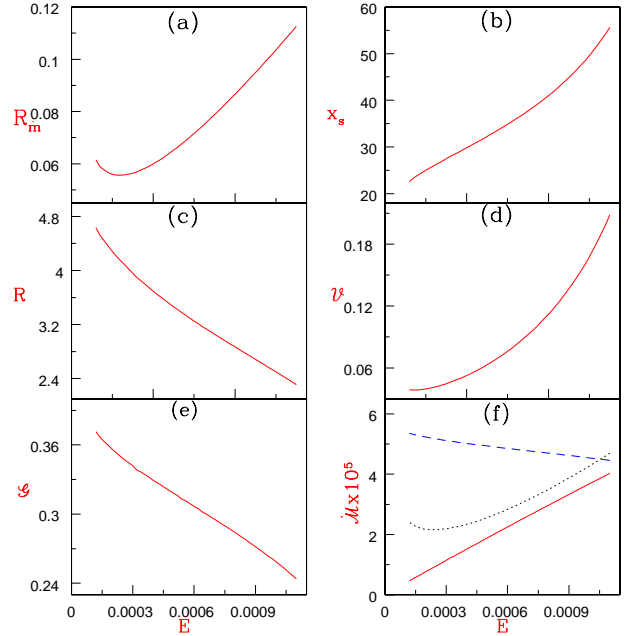


Figure 8. Various shock and jet quantities like R_m (a), x_s (b), R (c), ν (d), \mathcal{G} (e), and \dot{M} (f) are plotted with E for $\alpha = 0.05$ and $\lambda_0 = 1.54$.

the same outer boundary condition, x_s shifts closer to the horizon with the increase in α . Although, the viscosity prescription of Chattopadhyay & Das (2007) and the simulations are different, namely the former chose the stress to be proportional to total pressure, while in simulations the stress is proportional to the shear, still viscosity reduces angular momentum, and we know for lower angular momentum if the shock forms, it should form closer to the black hole! Since the viscosity prescription in this paper is similar to the simulations, we should be able to answer the dichotomy. So a concrete question may arise, if viscosity is increased, does the x_s expands to larger distances or, contracts to a position closer to the horizon? If the viscosity acts in a way such that the λ_+ (immediate post-shock λ) is less than its inviscid value at the shock then x_s will move closer to the horizon. However, such simple minded reasoning may fail, if shocks exists, then the post shock flow being hotter would transport more efficiently than the immediate pre-shock flow. So although, $\lambda_- < \lambda(x_{inj})$, it is not necessary λ_+ will be less than $\lambda(x_{inj})$. We scoured the parameter space to find the answer, and in the following we present the explanation.

Let x_b be the distance at which the λ distribution of the viscous solution is coincident with the λ value of the inviscid solution, let us further assign $\lambda_b = \lambda(x_b)$. It is to be remembered that $\lambda_0 = \lambda_b$ for the inviscid ($\alpha = 0$) solution, but $\lambda_0 < \lambda_b$ for viscous solution because viscosity reduces the angular momentum. In all the simulations done on viscous flow in the advective regime referred in this paper, one starts with an inviscid solution (since analytical solutions are readily available), and then the viscosity is turned on, keeping the values at the outer boundary fixed. In other words, it is this x_b that is called the outer boundary in numerical simulations, and generally, $x_b \lesssim \text{few} \times 100$ since it is computationally expensive to simulate a large domain from just outside the horizon to $\text{few} \times 1000 r_g$ and still retain required resolu-

tion to achieve intricate structures in the accretion disc. In Figs. 5a-c, we compare the $\lambda(x)$ of shocked accretion flows starting with the same $E = 10^{-4}$, & $\lambda_b = 1.68$ for various viscosity parameters such as, $\alpha = 0$ (solid), $\alpha = 0.0075$ (dotted), $\alpha = 0.015$, but for different points of coincidence, e.g., $x_b = 2220$ (5a), $x_b = 3660$ (5b), and $x_b = 5230$ (5c). The vertical solid line is the location of the shock for the inviscid flow. Although, we match the λ_b at x_b of the viscous and inviscid solutions, we still integrate outwards upto $x_{inj} = 10^4$. Since $x_{inj} \gg 1$, this distance may be considered as the size of the disc. In Figs. 5a-c, we show that depending upon the choice of x_b , the outer boundary conditions can be remarkably different. If x_b is short (Fig. 5a), then flow with higher α will be able to match λ_b at the same x_b , only if one starts with much higher λ_{inj} , in other words the gradients will be stiffer. Consequently, the increase of α will create higher λ_+ , which will result in the increase of x_s . In case x_b is large (Fig. 5c), the gradients are smoother and the resulting λ_{inj} will be approximately similar for any value of α . Hence as α is increased, λ_+ would decrease and consequently x_s will decrease too. In Fig. 5a, the parameters are $\lambda_{inj} = \lambda_b = 1.68$ for inviscid or $\alpha = 0$ (solid), $\lambda_{inj} = 1.769$ for $\alpha = 0.0075$ (dotted) and $\lambda_{inj} = 1.858$ for $\alpha = 0.015$ (dashed). Since $x_b = 2220$ is short, the gradients are steeper, and as discussed above, in such cases x_s increases with increasing α . While in Fig. 5c, $\lambda_{inj} = 1.744$ for $\alpha = 0.0075$ (dotted) and $\lambda_{inj} = 1.807$ for $\alpha = 0.015$ (dashed), where $x_b = 5230$ is larger, the shock x_s decreases with increasing α . Since for shorter values of x_b , x_s increases with the increase of α , and for longer x_b , x_s decreases with the increase of α , so a limiting x_b should exist for which x_s will neither increase or decrease with the increase of α . In Fig. 5b, we show that for $x_b = 3660$, the shock neither increase or decrease with the increase of α .

In Figs. 5d & e, we plot the limiting x_b as a function of E for $\lambda_0 = 1.68$ (d) and $\lambda_0 = 1.65$ (e). The domain name ‘1’ corresponds to any x_b at which the x_s will decrease and ‘2’ signifies the domain where at any x_b , x_s increases with α . Hence Fig. 5a lies in domain 2, Fig. 5b on the curve, and Fig. 5c on domain 1 of Fig. 5d. Incidentally, if the outer boundary condition for all the advective solutions start with the Keplerian angular momentum, then the shock location x_s decreases with the increase of α . Since the numerical simulations are usually performed with a shorter radial extent ($x_b \sim \text{few} \times 10 - \text{few} \times 100$), this is similar to the case x_b lying in the domain 2. As a result, earlier simulations of advective accretion flows have reported the increase of x_s with the increase of α . Hence we may conclude that the increment of x_s with the increase of α is an artifact of faulty assignment of outer boundary condition in the simulations.

In Fig. 6, the $E - \lambda_0$ parameter space for standing accretion shock has been plotted for various viscosity parameters, $\alpha = 0, 0.05, 0.1, 0.15, 0.2, 0.25, 0.3$. Since viscosity will in general reduce the angular momentum along the flow, λ_0 should decrease with the increase of α . As a result, the shock parameter space shift to the lower end of the λ_0 scale. One may compare the RH shock parameter space with that of the isothermal shock space (Das *et al.* 2009). For all possible boundary conditions, RH shocks may be obtained upto $\alpha = 0.3$. For values outside the bounded regions there are no standing shocks, although transient and oscillating shocks may exist. It is to be remembered though, the pa-

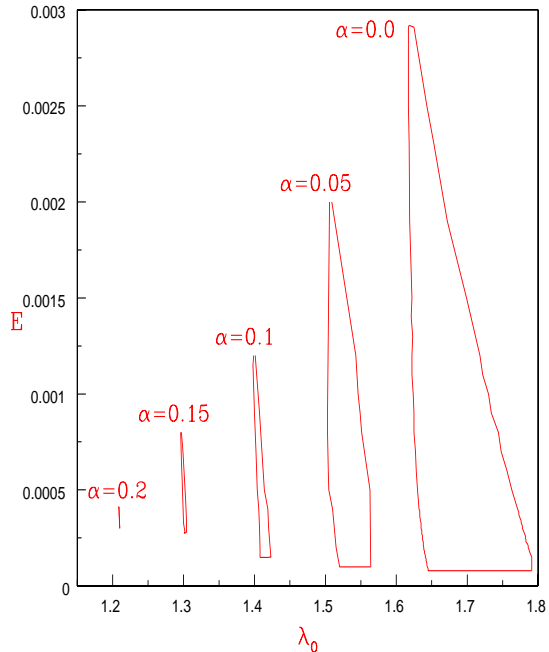


Figure 9. $E - \lambda_0$ parameter space of the standing adiabatic shock with Shakura-Sunyaev viscosity parameter $\alpha = 0.0, 0.05, 0.1, 0.15, 0.2$ marked on the figure, and in presence of massloss.

parameter space shown here corresponds to inner boundary. In the outer boundary λ might be much higher for viscous flow as has been shown in Figs. 4a-e.

4.2 Inflow-Outflow solutions

In the previous sub-section we discussed all possible solutions that one can have in presence of viscosity prescription given by Eq. (6), and non-dissipative or RH shocks. In this section we present the self consistent inflow-outflow solutions. In presence of massloss, the mass conservation equation across the shock will be modified in the form of Eq. (34). All the steps mentioned in section 3.2 are followed to compute the self-consistent inflow-outflow solution. In Fig. 7a-d, we present one case of global accretion-ejection solution. In Fig. 7a, the accretion solution in terms of $M(x)$ or the Mach number is presented, in Fig. 7b, the jet Mach number M_j is plotted with the height y_j of the jet from the equatorial plane of the disc, where the radial coordinate of the jet is $r_j = \sqrt{x_j^2 + y_j^2}$. The sonic points are marked with open circles. The inner boundary for the accretion solution is $E = 0.001$, $\lambda_0 = 1.542$. The specific energy and the angular momentum at the shock are $\mathcal{E}_+ = 1.084 \times 10^{-3}$, $\lambda_+ = 1.699$. The collimation parameter of the jet (see, Chattopadhyay 2005) at its sonic point is $x_{jc}/y_{jc} \sim 0.24$, and hence the spread is quite moderate. The dotted vertical line is the position of the shock when $R_{in} = 0$, and the solid vertical line is the position of the shock after the mass-outflow rate has been computed. Clearly, since excess thermal gradient force in the post-shock disc drives bipolar outflows, it reduces the

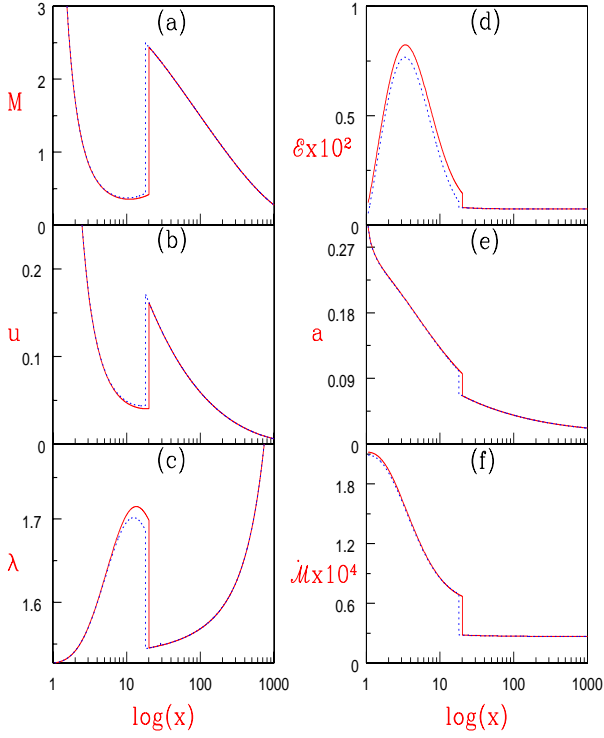


Figure 10. Comparison of accretion solutions with non-dissipative shock *i.e.*, $f_e = 0$ (solid), and dissipative shock $f_e = 0.1$ (dotted). The inner boundary condition for $f_e = 0$ are E , $\lambda_0 = 7.373 \times 10^{-4}$, 1.527 (solid), and for $f_e = 0.1$ are E_+ , $\lambda_0 = 2.5 \times 10^{-4}$, 1.527 (dotted). In case of the dotted curve $E_- = 7.373 \times 10^{-4}$. For $f_e = 0$, $x_s = 20.15$, & $R_{\dot{m}} = 0.1133$ (solid), and for $f_e = 0.1$, $x_s = 18.04$ & $R_{\dot{m}} = 0.0755$ (dashed). Various flow variables are M (a), u (b), λ (c), \mathcal{E} (d), a (e), and \dot{M} (f).

pressure, and hence to maintain the total pressure balance across the shock, the shock front moves closer to the horizon. The relative mass outflow rate computed for the particular case depicted in Figs. 7a-d, is $R_{\dot{m}} = 0.1044$. In Fig. 7c, we plot the density ρ_j of the jet derived for $\dot{M} = 0.1M_{\text{Edd}}$ for a black hole of $M = 10M_{\odot}$. In Fig. 7d, we plot the temperature T_j of the jet. As is expected the jet is hot near its base but falls to low temperatures at larger distances away, while the density also falls as is expected of a transonic jet.

Figures 8a-f, are plotted for the fixed values of $\alpha = 0.05$ and $\lambda_0 = 1.54$. Various quantities $R_{\dot{m}}$ (a), x_s (b), R (c), \mathcal{V} (d), \mathcal{G} (e), and \dot{M} (f) are plotted with E , which means, we are studying how $R_{\dot{m}}$ change with the change of inner boundary condition. Generally the $R_{\dot{m}}$ is few percent of the injected accretion rate but it can go upto more than 10% of \dot{M}_- for high E . Although in this plot, our main interest is to quantify the relative mass outflow rate $R_{\dot{m}}$ with E for given value of α and λ_0 , we have plotted all the essential quantities that would contribute in driving a part of the post-shock matter as outflows. The shock location x_s increases with the increase of E , and for increasing x_s , R should decrease. Since $R_{\dot{m}}$ is combination of R , \mathcal{V} and \mathcal{G} , even for falling R and \mathcal{G} , the mass outflow rate increases since it is being compensated by the increase of \mathcal{V} . Interestingly, none of the quantities show a monotonic variation. It is important to

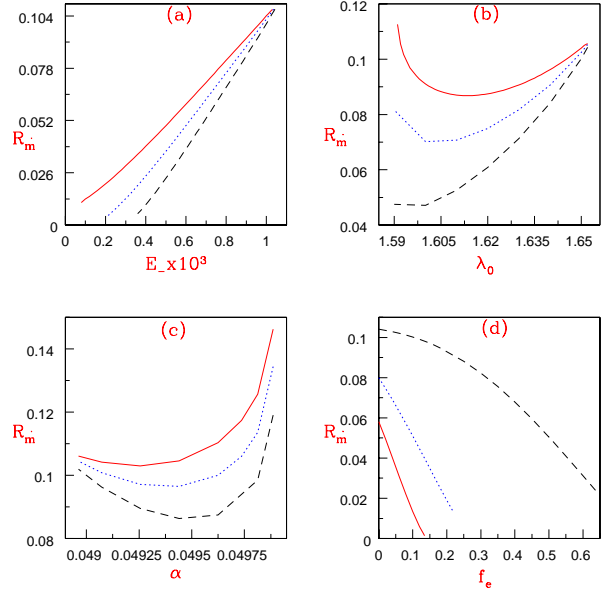


Figure 11. Relative mass outflow rate $R_{\dot{m}}$ as a function of (a) E_- for fixed values of $\alpha = 0.02$, $\lambda_0 = 1.65$; (b) λ_0 for fixed values of $E_- = 0.001$ and $\alpha = 0.02$; (c) α for fixed values of $E_- = 0.001$ and $\lambda_{inj} = 70.6$ at $x_{inj} = 10^4$; where all the plots are for $f_e = 0$ (solid), $f_e = 0.05$ (dotted) and $f_e = 0.1$ (dashed). (d) $R_{\dot{m}}$ as a function of f_e for fixed values of $E_- = 0.001$ and $\lambda_0 = 1.65$ and each curves are for $\alpha = 0$ (solid), $\alpha = 0.01$ (dotted) and $\alpha = 0.02$ (dashed).

note, all the three parameters R , \mathcal{V} and \mathcal{G} represent the jet to disc connection and not the actual driving. The real drivers are however, the post-shock specific energy \mathcal{E}_+ , and the jet base cross-section $\mathcal{A}_s (\equiv \mathcal{A}(x_s))$. Higher \mathcal{E}_+ means hotter flow at the jet base, and therefore the thermal driving will be more. This is complemented by the cross-section \mathcal{A}_s of the jet base. Higher \mathcal{E}_+ would drive more matter into the jet channel but will be limited by the cross-sectional area. In Fig. 8f, we plot the pre-shock entropy-accretion rate \dot{M}_- (solid), the post-shock entropy-accretion rate \dot{M}_+ (dashed) and the jet entropy-accretion rate \dot{M}_j (dotted), as a function of E , and it is quite evident that the pre-shock entropy is less than both \dot{M}_j and \dot{M}_+ . Moreover, when the value of \dot{M}_j is high, $R_{\dot{m}}$ is found to be high too, which vindicates that matter would prefer to flow through channels with higher entropy.

From Eq. (34), we know that $\dot{M}_+ < \dot{M}_-$ if $R_{\dot{m}} \neq 0$. Therefore, the post-shock pressure would be reduced. This would cause x_s to decrease as shown in Fig. 7a [also see Chattopadhyay & Das (2007)]. Furthermore, the massloss from the post-shock flow and consequent reduction in pressure would also modify shock parameter space. In Fig. 9, the bounded regions in the $E - \lambda_0$ space, represents the shock parameter space for $\alpha = 0, 0.05, 0.1, 0.15$ and 0.2 , marked on the figure. Compared to the shock parameter space in absence of massloss (Fig. 6), the parameter space in presence of massloss gets reduced and beyond $\alpha = 0.2$ the standing shock seems to vanish. Moreover, the shock parameter space shows that the standing shock do not seem to exist for very low E . Non-existence of standing shock ofcourse do not imply non-existence of non-steady or oscillatory shocks.

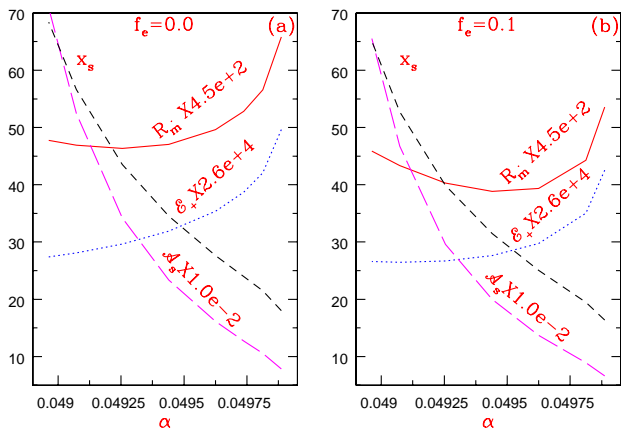


Figure 12. Relative mass outflow rate $R_{\dot{m}}$ (solid), x_s (dashed), \mathcal{E}_+ (dotted), and \mathcal{A}_s (long-dashed) as a function of α for $f_e = 0$ (a) and $f_e = 0.1$ (b) for fixed values of $E_- = 0.001$ and $\lambda_{inj} = \lambda_K(x_{inj}) = 70.6$ at $x_{inj} = 10^4$.

4.3 Massloss from the dissipative shocks

Chakrabarti & Titarchuk (1995) and later Mandal & Chakrabarti (2010) had shown that the post shock hot flows can produce the high energy photons easily by inverse-Comptonizing the soft photons and reproduced the observed spectra from variety of objects. If indeed the observed spectra and luminosity can be reproduced from the post-shock flow, then the grand energy will not be conserved across the shock and will be given by Eq. (36), and the dissipated energy can be radiated away. In Fig. 10a-f, various flow variables M (a), u (b), λ (c), \mathcal{E} (d), a (e), and \dot{M} (f) are plotted for $f_e = 0$ (solid) and $f_e = 0.1$ (dotted). For $f_e = 0$ (solid), the solutions are plotted for flow parameters E , $\lambda_0 = 7.373 \times 10^{-4}$, 1.527. For $f_e = 0$, we have $E = E_+ = E_-$. However, for $f_e > 0$, $E_+ < E_-$. So for $f_e = 0.1$ (dotted), the inner boundary is represented by E_+ , $\lambda_0 = 2.5 \times 10^{-4}$, 1.527, while the pre-shock $E_- = 7.373 \times 10^{-4}$. The post-shock specific energy or Bernoulli parameter, temperature, angular momentum, and entropy of the solution with dissipative shock (dotted) are lower than those corresponding to the non-dissipative shock (solid). Since a part of the thermal energy gained through shock is spent in powering jets and to produce radiation, the shock front moves closer to the black hole. The relative mass outflow rate or $R_{\dot{m}}$ is lower for dissipative shocks, because part of the thermal energy of the post-shock disc is lost through radiation. However, the thermal energy lost as radiation can still contribute to jet power if those photons deposit momentum onto the jets (Chattopadhyay & Chakrabarti 2002; Chattopadhyay *et al.* 2004; Chattopadhyay 2005).

If $f_e \neq 0$ and shocks are present, then the accretion solutions are obtained either for E_+ , λ_0 , α , f_e , or equiva-

lently, E_- , λ_0 , α , f_e , or, E_- , λ_{inj} , α , f_e . If $f_e = 0$ then $E = E_+ = E_-$, therefore any of the following two sets would suffice E , λ_0 , α , or, E , λ_{inj} , α . Since the outflows are launched from the post-shock flow, the mass outflow rates are computed only from the shocked accretion flows, and we are interested to find the dependence of $R_{\dot{m}}$ on each of the above mentioned parameters. In Fig. 11a, we plot $R_{\dot{m}}$ as a function of E_- when the other parameters are fixed at $\alpha = 0.02$, $\lambda_0 = 1.65$ where each of the curve are for $f_e = 0$ (solid), $f_e = 0.05$ (dotted) and $f_e = 0.1$ (dashed). With the increase of E_- , the post-shock specific energy \mathcal{E}_+ increases which drives more matter as outflow, and hence $R_{\dot{m}}$ increases. However, for any given E_- , $R_{\dot{m}}$ decrease with the increase of f_e , *i.e.*, the mass outflow decreases with the increase of the thermal energy dissipation. Although for very high E_- , the separation of the curves decreases, this shows that flows starting with higher energy would have enough thermal energy to drive significant outflows even for $f_e \neq 0$. Now, let us fix E_- but vary λ_0 in Fig. 11b. $R_{\dot{m}}$ is plotted with λ_0 for $f_e = 0$ (solid), $f_e = 0.05$ (dotted) and $f_e = 0.1$ (dashed). The fixed parameters are $E_- = 0.001$, and $\alpha = 0.02$, and clearly $R_{\dot{m}}$ is not a monotonic function of λ_0 . Increasing λ_0 would increase λ_+ and therefore increase x_s but would decrease \mathcal{E}_+ . The increase of x_s , increases the jet base cross-section. The competition between \mathcal{E}_+ and \mathcal{A}_s causes a dip in $R_{\dot{m}}$ for moderate values of λ_0 .

However, $R_{\dot{m}}$ decreases with the increase of f_e . In Fig. 11c, we fix the outer boundary condition, namely, $E_- = 0.001$, $\lambda_{inj} = 70.6$ at $x_{inj} = 10^4$, and $R_{\dot{m}}$ is plotted as a function of α , where each of the curves are for $f_e = 0$ (solid), $f_e = 0.05$ (dotted) and $f_e = 0.1$ (dashed). Since for flows starting with such high λ_{inj} there would be no accretion shock solution for low α , therefore one observes outflows only beyond a critical value of α . We know (see Fig. 5c) that for flow starting with the same outer boundary condition, the shock location decreases with the increasing α . Decrease in x_s would mean decrease in \mathcal{A}_s . Since x_s decreases, it means the post-shock energy increases due to viscous dissipation *i.e.*, \mathcal{E}_+ increases. Increase in \mathcal{E}_+ would drive more matter into the outflow channel. Therefore, the decrease in \mathcal{A}_s is dominated by the increase in \mathcal{E}_+ , and so $R_{\dot{m}}$ increases with α for a fixed outer boundary condition.

However, $R_{\dot{m}}$ decreases with the increase in f_e , which also shows that these jets are thermally driven. In Fig. 11d, $R_{\dot{m}}$ is plotted with f_e for $\alpha = 0$ (solid), $\alpha = 0.01$ (dotted) and $\alpha = 0.02$ (dashed). The fixed parameters are $E_- = 0.001$ and $\lambda_0 = 1.65$. It was also found out that there are critical f_e beyond which no standing shock conditions are satisfied, and they are $f_{ec} = 0.135$ for $\alpha = 0$ (solid), $f_{ec} = 0.22$ for $\alpha = 0.05$ (dotted) and $f_{ec} = 0.645$ for $\alpha = 0.1$ (dashed). It is obvious that f_{ec} increases with the increase of α .

It is to be noted that $R_{\dot{m}}$ is the fraction of matter which is shock heated and ejected out as bipolar outflows. To properly understand the role of shock in driving bipolar outflow, we consider accretion solutions with the same outer boundary condition, or the case presented in Fig. 11c. In Fig. 12a, we plot various quantities across the shock *e.g.*, $R_{\dot{m}}$ (solid), \mathcal{E}_+ (dotted), x_s (dashed), and \mathcal{A}_s (long dashed), as a function of α , and for $f_e = 0$, *i.e.*, corresponding to the solid plot of Fig. 11c. In Fig. 12b, we plot $R_{\dot{m}}$ (solid), \mathcal{E}_+ (dotted), x_s (dashed), and \mathcal{A}_s (long dashed), as a function of α , and

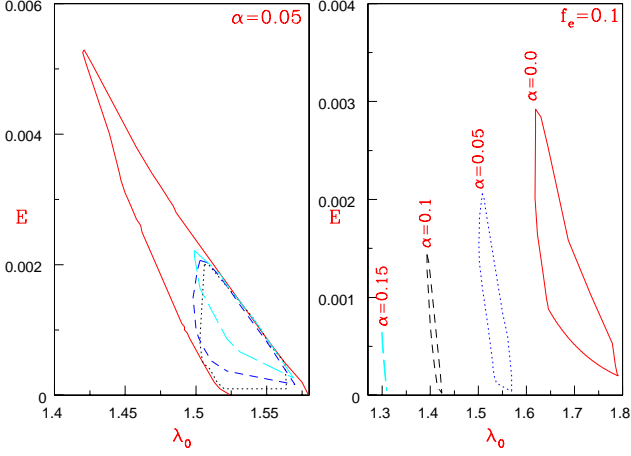


Figure 13. $E - \lambda_0$ shock parameter space for (a) $\alpha = 0.05$, and each curve is for $f = 1$, $f_e = 0$ (solid), $f > 1$, $f_e = 0$ (dotted), $f > 1$, $f_e = 0.05$ (dashed), and $f > 1$, $f_e = 0.2$ (long dashed), and (b) $f > 1$, $f_e = 0.1$, and each curve is for $\alpha = 0.0$ (solid), 0.05 (dotted), 0.1 (dashed), and 0.15 (long dashed).

for $f_e = 0.1$, *i.e.*, corresponding to the dashed plot of Fig. 11c. Increasing α in accretion with the same outer boundary condition, will decrease λ_+ and therefore decrease x_s (dashed). Decrease in x_s implies that the shock is formed closer to the black hole, where the viscous dissipation would be more *i.e.*, \mathcal{E}_+ will be higher (dotted). The jet velocity is small at the jet base, so large \mathcal{E}_+ means hotter flow and stronger driving of the outflow *i.e.*, higher R_m . Figure 12b shows that, as the shock dissipation f_e is increased, at certain α , \mathcal{E}_+ is reduced while the decrease in \mathcal{A}_s is marginal, this causes R_m initially to decrease with α , but eventually starts to increase as \mathcal{E} increases appreciably.

In Fig. 13a, we plot the $E - \lambda_0$ shock parameter space for flows with $f = 1$, $f_e = 0$ (solid), $f > 1$, $f_e = 0$ (dotted), $f > 1$, $f_e = 0.05$ (dashed), and $f > 1$, $f_e = 0.2$ (long dashed). The viscosity parameter for this figure is $\alpha = 0.05$. It is to be remembered $f = 1$ means no massloss and $f > 1$ means presence of bipolar outflows. Therefore $f = 1$, $f_e = 0$ (solid), implies the shock parameter space for RH shocks with no massloss and no dissipation at the shock, while $f > 1$, $f_e = 0$ (dotted) implies non dissipative shock but massloss is present. Similarly, $f > 1$, $f_e = 0.05$ (dashed) and $f > 1$, $f_e = 0.2$ (long dashed) shock parameter space for dissipative shocks of various strength and in presence of massloss. The parameter space for standing shock shrinks with the increase of f_e . In Fig. 13b, we plot the shock parameter space for fixed $f_e = 0.1$ and various values of $\alpha = 0$ (solid), 0.05 (dotted), 0.1 (dashed) and 0.15 (long dashed). We know from Fig. 6, that with the increase of α the shock parameter space shrinks, however, in presence of massloss, flows with low E seems to show no standing shock. In Fig. 13b, we see that although the parameter space for shock shrinks but low E flow again exhibit standing

shock, which signifies that the mass outflow rate decreases with the increase of f_e .

5 DISCUSSION AND CONCLUSION

Quasars and micro-quasars may show strong jets, and these outflows are correlated with the spectral state of the object. Therefore, quantitative estimate of the generation of these outflows are required, especially, the relation between the mass outflow rates and the viscosity parameter needs to be ascertained, this is because the viscosity will determine the disc spectral states. Most of these estimates are available for inviscid flow, or special viscosity prescription or shock condition, but not for the most general shock condition, *i.e.*, partially dissipative shock.

In this paper, our main concern has been to estimate the thermally driven bipolar outflows from shocked accretion discs around black holes. Since accretion disc should possess some amount of viscosity, a proper understanding of viscous accretion disc is required. As outflows are generated from the post-shock disc and high energy photons should also emerge from the post-shock disc, an investigation of estimating the outflow rate and correlating it with the dissipation parameters is a must requirement. In order to estimate the outflows correctly, a proper understanding of the accretion process has to be undertaken, and we presented all possible accretion solutions without massloss in section 4.1, including the shocked and shock free accretion solutions and the dependence of these solutions on viscosity parameter. While doing so we have compared solutions with same inner and outer boundary conditions, and have shown that these differences produces a significant difference in interpreting the results.

For solutions with the same inner boundary conditions (*i.e.*, Figs. 3a-p), we found two critical viscosity parameters, the first one being the onset of shock (α_{cl}), and the other being the one above which standing shock disappears (α_{cu}) and generates a shock free global solution which is wholly subsonic except close to the horizon, or the ADAF type solution. Simultaneous existence of both α_{cl} and α_{cu} will depend on whether λ_0 is small enough to produce a corresponding O-type inviscid solution. If inviscid solution is already shocked then only α_{cu} will exist, while if the inviscid solution is I or W type then neither α_{cl} nor α_{cu} exists. For solutions with the same outer boundary condition, *i.e.*, flow starting with same E , $\lambda_{inj} = \lambda_K(x_{inj})$ at some injection radius x_{inj} , *e.g.*, Fig. 4a-e, there would be an additional critical viscosity parameter α_1 , which would allow a global solution connecting the horizon and the outer boundary x_{inj} . We have also confirmed that fluids in such cases, x_s would decrease with the increase of α . The decrease of x_s with the increase of α is interesting. Chakrabarti & Titarchuk (1995) for the first time argued that the post-shock disc is the elusive Compton cloud, which inverse-Comptonizes the pre-shock soft photons to produce power law tail. If the shock remains strong then we have the canonical hard state and when the shock becomes weak or disappear we have the canonical soft state. Moreover, Molteni *et al.* (1996b) showed that if the shock oscillates, it does with a frequency $\omega \sim x_s^{-\beta}$, where $\beta = 1 \rightarrow 3/2$. If the shock oscillates then the hard radiation from it would oscillate with the same frequency and could

explain the mHz to few tens of Hz QPO observed in stellar mass black hole candidates. Outburst phase in microquasars starts with low frequency QPOs in hard state, but as the source moves to intermediate states the QPO frequency increases to a maximum and then goes down in the declining phase, a fact well explained by approaching oscillating x_s with the increase of viscosity (Chakrabarti *et al.* 2009). Our steady state model also shows that if every other conditions at the outer boundary is same, then x_s decreases with the increase of α , so we expect with the increase of viscosity the shock oscillation too will increase, and therefore the shock oscillation model of QPO seems to follow observations.

We have computed the mass outflow rate from both non-dissipative as well as dissipative shocks. The mass outflow rate is always of higher entropy than the pre-shock disc, which shows that mass-outflow rate is a natural consequence of a shocked accretion disc, a fact readily supported by various multi-dimensional simulations. In this connection we would like to comment that unlike Chattopadhyay & Das (2007); Das & Chattopadhyay (2008), we have corrected the jet cross sectional area with the projection effect onto the jet streamline. We showed that R_{in} generally decreases with f_e . We also showed that the parameter space is significantly modified due to the presence of massloss and dissipation at the shock. When dissipative shocks are included we do see that the relative mass outflow rate decreases which are also to be expected. Increasing dissipation would make the shocks weaker, which can be identified with the softer spectral state, and the accretion disc in the soft state will give weaker or not outflow (Gallo *et al.* 2003).

Comparison of steady shock parameter space Figs. (6,9), suggests that massloss may trigger an instability. It shows that parts of parameter space which produced steady shocks in absence of massloss, do not show steady shocks in presence of massloss. This is because the post-shock pressure gets reduced as it loses mass, and the shock moves closer to the black hole (Fig. 7) to regain the momentum balance. However, this is not always possible, and the shock may oscillate or get disrupted altogether, therefore, there should be a massloss induced instability as well. We have also shown that the main driver for the bipolar outflow is the energy gained through shock. Interestingly, the mass outflow rate generally increase with the increasing viscosity parameter. Since the shock location also decreases with the increasing α for identical outer boundary condition, there is a possibility that the QPOs and mass outflow rates be correlated — an issue we will pursue in fully time dependent studies.

It is interesting to note that the dissipation parameter used in this work has been assumed constant, however this would actually depend on accretion rates and the size of the post-shock region. As the accretion rate changes the total photons generated would change, and similarly as x_s changes the fraction of photons intercepted by post-shock disc as well as its optical depth would change, this would render f_e variable.

It has been observationally established that steady jets are observed from black hole candidates, when the spectrum of the disc is in the hard state (Gallo *et al.* 2003). In our model, the presence of strong shock is similar to the hard state. We have shown that with the increasing α , we get stronger jet, however evolution of jet states with spec-

tral states is a time-dependent phenomenon. Moreover, the phenomena of QPO and growth or decay of QPO are time dependent phenomenon too. Our conjecture that the QPO will be correlated with the jet states can only be vindicated through a fully time dependent study, which is beyond the scope of this paper. Furthermore, since we concentrated on the effect of viscosity on accretion disc and outflows, therefore, magnetic field and other realistic cooling processes have been ignored. If cooling processes are considered then a direct comparison with the observation will be possible. As has been noted that a little bit of magnetic field will have an important effect on the dynamics of the flow (Proga 2005), however transonicity criteria will be important too. Because a magnetized flow may possess fast, slow or Alfvénic waves, and the number of sonic points may increase (Takahashi *et al.* 2006). If magnetized flows admit shocks, then the shock produced, may be even more robust. And this hydrodynamic model might well act as the simpler version of the magneto fluid model. We are working on dynamics of magnetized flows and would be reported elsewhere.

The concrete conclusions we draw from this paper is the following. Viscosity is important and affects the accretion solutions both quantitatively and qualitatively. Shock in accretion can be obtained for fairly high viscosity parameter. Shocks naturally produces outflows, and for fixed outer boundary conditions of the disc, shock location decreases but mass outflow rate generally increases. This augurs well for the model as this is exactly observed in hard to intermediate hard spectral transitions. However, in presence of dissipative shocks the mass outflow rate decreases. Over all we see that R_{in} may vary between few % to more than 10 %, although in presence of dissipative shocks, the estimate of R_{in} is about few %. We have also computed the shock parameter space for accreting flows without mass loss and dissipation, with massloss but no dissipation and with massloss and dissipation and have shown that the parameter space for steady shocks shrinks with increasing dissipation.

REFERENCES

- Aoki, S. I., Koide, S., Kudoh, T., Nakayama, K., 2004, ApJ, 610, 897
- Becker, P. A., Le, T., 2003, ApJ, 588, 408
- Becker, P. A., Subramaniam, P., 2005, ApJ, 622, 520
- Becker, P. A., Das, S., Le, T., 2008, ApJ, 677, L93
- Blandford, R. D., Znajek, R. L., 1977, MNRAS, 179, 433.
- Blandford, R. D., Payne, D. G., 1982, MNRAS, 199, 883.
- Blandford, R. D., Begelman, M. C. 1999, MNRAS, 303, L1
- Bondi, H., 1952, MNRAS, 112, 195
- Chen, X., Abramowicz, M., & Lasota, J.-P. 1997, ApJ, 476, 61
- Chakrabarti, S. K., 1989, ApJ, 347, 365
- Chakrabarti, S. K., 1990, 'Theory of Transonic Astrophysical Flows' by Sandip K. Chakrabarti, (Singapore, World Scientific Publishing Co. Ltd.).
- Chakrabarti, S. K., Titarchuk, L., 1995, ApJ, 455, 623.
- Chakrabarti, S. K., 1996, ApJ, 464, 664
- Chakrabarti, S. K., 1999, A&A, 351, 185
- Chakrabarti, S. K., Das, S., 2004, MNRAS, 349, 649
- Chakrabarti, S. K., Mandal, S., 2006, ApJ, 642, L49

- Chakrabarti, S. K., Dutta, B. G., Pal, P. S., 2009, MNRAS, 394, 1463
- Chattopadhyay, I., Chakrabarti, S. K., 2002, MNRAS, 333, 454.
- Chattopadhyay, I., Das, S., Chakrabarti, S. K., 2004, MNRAS, 348, 846.
- Chattopadhyay, I., 2005, MNRAS, 356, 145
- Chattopadhyay, I.; Das, S., 2007, New A, 12, 454
- Chattopadhyay, I., 2008, AIPC, 1053, 353.
- Chattopadhyay, I., Ryu, D., 2009, ApJ, 694, 492
- Chattopadhyay, I., Chakrabarti, S. K., 2011, IJMPD, 20, 1597
- Das, S., Chattopadhyay, I., Chakrabarti, S. K., 2001, A&A, 379, 683
- Das, S.; Chattopadhyay, I., 2008, New A, 13, 549D.
- Das, S.; Becker, P. A.; Le, T., 2009, ApJ, 702, 649
- Fender, R. P., Gallo, E., Russell, D., 2010, MNRAS, 406, 1425.
- Fukue, J., 1987, PASJ, 39, 309
- Fukumura, K., Tsuruta, S., 2004, ApJ, 611, 964
- Fukumura, K., Kazanas, D., 2007, ApJ, 669, 85
- Gallo, E., Fender, R. P., Pooley, G., G., 2003 MNRAS, 344, 60
- Gu, Wei-Min; Lu, Ju-Fu, 2004, ChPhL, 21, 2551
- Hawley, J. F., Beckwith, K., Krolik, J. H., 2007, Ap&SS, 311, 117
- Ichimaru, S. 1977, ApJ, 214, 8401
- Junor, W., Biretta, J. A., Livio, M., 1999, Nature, 401, 891
- Lanzafame, G., Molteni, D., Chakrabarti, S. K., 1998, MNRAS, 299, 799
- Lanzafame, G., Cassaro, P., Schilliró, F., Costa, V., Belvedere, G., Zappalá, R. A., 2008, A&A, 482, 473
- Liang, E. P. T., Thompson, K. A., 1980, ApJ240, 271L
- Le, T.; Becker, P. A., 2005, ApJ, 632, 476.
- Lee, S. J., Ryu, D., Chattopadhyay, I., 2011, ApJ, 728, 142.
- Lu, J. F., Gu, W. M., & Yuan, F. 1999, ApJ, 523, 340
- Mandal, S., Chakrabarti, S. K., 2008, ApJ, 689, L17.
- Mandal, S., Chakrabarti, S. K., 2010, ApJ, 710, L147.
- Matsumoto, R.; Kato, S.; Fukue, J.; Okazaki, A. T., 1984, PASJ, 36, 71
- Molteni, D., Lanzafame, G., Chakrabarti, S. K., 1994, ApJ, 425, 161
- Molteni, D., Ryu, D., Chakrabarti, S. K., 1996, ApJ, 470, 460
- Molteni, D., Sponholtz, H., Chakrabarti, S. K., 1996, ApJ, 457, 805
- Narayan, R., & Yi, I. 1994, ApJ, 428, L13
- Narayan, R., Kato, S., Honma, F., 1997, ApJ, 476, 49
- Nagakura, H., Yamada, S., 2008, ApJ, 689, 391
- Nagakura, H., Yamada, S., 2009, ApJ, 696, 2026
- Novikov, I. D.; Thorne, K. S., 1973, blho, conf, 343.
- Nishikawa, K. -I., Richardson, G., Koide, S., Shibata, K., 2005, ApJ, 625, 60
- Paczynski, B. and Wiita, P.J., 1980, A&A, 88, 23.
- Proga, D., 2005, ApJ, 629, 397
- Shakura, N. I.; Sunyaev, R. A., 1973, A&A, 24, 337S.
- Singh, C. B., Chakrabarti, S. K., 2012, MNRAS, 421, 1666
- Smith, D. M., Heindl, W. A., Markwardt, C. B., Swank, J. H., 2001, ApJ, 554, L41
- Smith, D. M., Heindl, W. A., Swank, J. H., 2002, ApJ, 569, 362
- Takahashi, M., Goto, J., Fukumura, K., Rillet, D., Tsuruta, S., 2006, ApJ, 645, 1408
- Weinberg, S., 1972, Gravitation and Cosmology (New York: Willey)